Climbing up the Ladder: Intermediate Triplet States Promote the Reverse Intersystem Crossing in the Efficient TADF Emitter ACRSA

Supporting Information

Igor Lyskov and Christel M. Marian*

Institute of Theoretical and Computational Chemistry,
Heinrich-Heine-University Düsseldorf, Universitätsstraße 1,
40225 Düsseldorf, Germany,
E-mail: Christel.Marian@hhu.de

August 30, 2017

Table S1: Vertical electronic excitation energies (eV) at the ground-state geometry as a function of the AO basis and DFT/MRCI parameter set. Note that some values may be different from those in the main text of the article due to slightly modified reference space.

State	Character[a–e]	Excitation	SV(P) basis		TZVP basis		cc-aug-pTZV[f]	
			DFT/MRCI-R		DFT/MRCI-R		DFT/MRCI-R	
			standard	tight	standard	tight	standard	tight
1^1A_1		ground state	0.00	0.00	0.00	0.00	0.00	0.00
1^1A_2	CT / ANT	$\pi_{\mathrm{H}} \rightarrow \pi^*_{\mathrm{L}}$ / $n_{\mathrm{O}} \rightarrow \pi^*_{\mathrm{L}}$	3.37	3.40	3.32	3.36	3.32	3.36
2^1A_2	ANT / CT	$n_{\mathrm{O}} \rightarrow \pi^*_{\mathrm{L}}$ / $\pi_{\mathrm{H}} \rightarrow \pi^*_{\mathrm{L}}$	3.53	3.55	3.55	3.57	3.55	3.58
1^1B_1	CT / ANT	$\pi_{\mathrm{H-1}} \rightarrow \pi^*_{\mathrm{L}}$	3.96	3.96	3.94	3.95	3.95	3.99
1^1B_2	ACR / CT*	$\pi_{\mathrm{H}} \rightarrow \pi^*_{\mathrm{L+1}}$	4.01	4.02	3.99	4.01	3.96	3.99
2^1A_1	ACR	$\pi_{\mathrm{H}} \rightarrow \pi^*_{\mathrm{L+4}}$	4.07	4.07	4.04	4.06	4.02	4.05
3^1A_1	ANT	$\pi_{\mathrm{H-3}} \rightarrow \pi^*_{\mathrm{L}}$	4.17	4.14	4.18	4.17	4.18	4.21
1^3A_2	ANT / CT	$n_{\mathrm{O}} \rightarrow \pi^*_{\mathrm{L}}$ / $\pi_{\mathrm{H}} \rightarrow \pi^*_{\mathrm{L}}$	3.23	3.24	3.22	3.25	3.24	3.27
1^3B_2	ACR	$\pi_{\mathrm{H}} \rightarrow \pi^*_{\mathrm{L+1}}$	3.33	3.30	3.35	3.34	3.36	3.35
1^3A_1	ANT	$\pi_{\mathrm{H-6}} \rightarrow \pi^*_{\mathrm{L}}$	3.39	3.37	3.37	3.40	3.47	3.46
2^3A_2	CT / ANT	$\pi_{\mathrm{H}} \rightarrow \pi^*_{\mathrm{L}}$ / $n_{\mathrm{O}} \rightarrow \pi^*_{\mathrm{L}}$	3.40	3.40	3.43	3.41	3.38	3.42
1^3B_1	ACR/CT	$\pi_{\mathrm{H-4}} \rightarrow \pi^*_{\mathrm{L}}$ / $\pi_{\mathrm{H-5}} \rightarrow \pi^*_{\mathrm{L}}$	3.48	3.44	3.49	3.46	3.53	3.51
2^3B_1	CT / ANT	$\pi_{\mathrm{H-1}} \rightarrow \pi^*_{\mathrm{L}}$	3.64	3.58	3.62	3.58	3.65	3.63
2^3A_1	ACR	$\pi_{\mathrm{H}} \rightarrow \pi^*_{\mathrm{L+4}}$	3.67	3.62	3.64	3.60	3.60	3.56
3^3A_1	ANT/ACR	$\pi_{\mathrm{H-3}} \rightarrow \pi^*_{\mathrm{L}}$ / $\pi_{\mathrm{H-1}} \rightarrow \pi^*_{\mathrm{L+1}}$	3.77	3.72	3.78	3.74	3.80	3.77
2^3B_2	ACR/CT*	$\pi_{\mathrm{H}} \rightarrow \pi^*_{\mathrm{L+7}}$ / $\pi_{\mathrm{H}} \rightarrow \pi^*_{\mathrm{L+3}}$	3.82	3.74	3.79	3.74	3.79	3.75
4^3A_1	ACR/ANT	$\pi_{\mathrm{H-2}} \rightarrow \pi^*_{\mathrm{L+4}}$/ $\pi_{\mathrm{H-3}} \rightarrow \pi^*_{\mathrm{L}}$/ $\pi_{\mathrm{H}} \rightarrow \pi^*_{\mathrm{L+9}}$	3.85	3.79	3.87	3.83	3.88	3.84
5^3A_1	PHE	$\pi_{\mathrm{H-8}} \rightarrow \pi^*_{\mathrm{L+3}}$/ $\pi_{\mathrm{H-7}} \rightarrow \pi^*_{\mathrm{L+2}}$	4.02	3.93	4.03	3.97	3.80	3.99
3^3B_2	ACR	$\pi_{\mathrm{H-1}} \rightarrow \pi^*_{\mathrm{L+4}}$	4.03	3.98	4.05	4.01	4.05	4.02
3^3B_1	ANT	$\pi_{\mathrm{H-1}} \rightarrow \pi^*_{\mathrm{L+5}}$	4.07	4.01	4.09	4.03	4.11	4.07

[a]: ANT = local excitation on the anthracenone moiety
[b]: CT = charge transfer from acridine to anthracenone
[c]: ACR = local excitation on the acridine moiety
[d]: CT* = charge transfer from acridine to the phenyl ring
[e]: PHE = local excitation on the phenyl moiety
[f]: cc-aug-pTZV basis for O, N, C, cc-pDZV basis for H.

Table S2: Adiabatic excitation energies ΔE_{adia} (eV), vertical emission energies ΔE_{em} (eV) and static dipole moments μ (Debye) of low-lying electronic states of ACRSA (def-SV(P) basis set) in vacuum.

State	Character	Excitation	ΔE_{adia}	ΔE_{em}	μ
1^1A_1		(0.96) GS	0.00	—	5.46
1^1A_2	ANT	(0.79) $n_O \rightarrow \pi^*_L$	3.12	2.76	2.13
2^1A_2	CT	(0.80) $\pi_H \rightarrow \pi^*_L$	3.14	3.04	19.60
1^1B_1	CT / ANT	(0.72) $\pi_{H-1} \rightarrow \pi^*_L$	3.87	3.67	10.62
2^1A_1	ACR	(0.72) $\pi_H \rightarrow \pi^*_{L+4}$	4.02	3.88	6.83
1^1B_2	ACR / CT*	(0.71) $\pi_H \rightarrow \pi^*_{L+1}$	4.07	3.79	2.74
1^3A_2	ANT	(0.81) $n_O \rightarrow \pi^*_L$	2.96	2.57	1.98
2^3A_2	CT / ANT	(0.59) $\pi_H \rightarrow \pi^*_L$ (0.25) $n_O \rightarrow \pi^*_L$	3.13	2.93	14.94
1^3B_2	ACR/CT	(0.65) $\pi_H \rightarrow \pi^*_{L+1}$	3.14	2.93	7.00
1^3A_1	ANT	(0.82) $\pi_{H-6} \rightarrow \pi^*_L$	3.24	2.12	3.48
1^3B_1	ACR/CT	(0.38) $\pi_{H-4} \rightarrow \pi^*_L$ (0.31) $\pi_{H-1} \rightarrow \pi^*_L$	3.34	3.11	6.97

[a]: ANT = local excitation on the anthracenone moiety
[b]: CT = charge transfer from acridine to anthracenone
[c]: ACR = local excitation on the acridine moiety
[d]: CT* = charge transfer from acridine to the phenyl ring

Table S3: Important spin–orbit coupling matrix elements[a] (cm^{-1}) of DFT/MRCI wave functions (def-SV(P) basis set, tight) at various molecular geometries.

	Geometry				
	GS	^{1}CT	^{3}CT	$^1(n\pi^*)$	$^3(n\pi^*)$
$\langle 1^3A_2\|\hat{\mathcal{H}}_{\mathrm{SO\ z}}\|1^1A_1\rangle$	–34.03	–21.47	–23.01	–44.64	–44.98
$\langle 2^3A_2\|\hat{\mathcal{H}}_{\mathrm{SO\ z}}\|1^1A_1\rangle$	25.38	–37.80	36.93	6.52	6.44
$\langle 1^3A_1\|\hat{\mathcal{H}}_{\mathrm{SO\ z}}\|1^1A_2\rangle$	–15.98	–11.51	12.33	43.70	–44.25
$\langle 1^3A_1\|\hat{\mathcal{H}}_{\mathrm{SO\ z}}\|2^1A_2\rangle$	–23.68	–33.51	–33.39	–3.51	–3.40
$\langle 1^3B_1\|\hat{\mathcal{H}}_{\mathrm{SO\ x}}\|1^1A_2\rangle$	– 0.80	–0.53	–0.55	–1.20	–1.20
$\langle 1^3B_1\|\hat{\mathcal{H}}_{\mathrm{SO\ x}}\|2^1A_2\rangle$	1.10	1.26	1.25	–0.02	–0.00
$\langle 1^3B_2\|\hat{\mathcal{H}}_{\mathrm{SO\ y}}\|1^1A_2\rangle$	0.61	0.66	–0.67	–0.13	–0.12
$\langle 1^3B_2\|\hat{\mathcal{H}}_{\mathrm{SO\ y}}\|2^1A_2\rangle$	0.32	–0.15	–0.17	–0.74	–0.73
$\langle 1^3A_2\|\hat{\mathcal{H}}_{\mathrm{SO\ z}}\|1^3A_1\rangle$	–23.08	–19.07	20.32	42.63	43.19
$\langle 2^3A_2\|\hat{\mathcal{H}}_{\mathrm{SO\ z}}\|1^3A_1\rangle$	16.61	28.41	–27.73	–3.19	–3.12
$\langle 1^3B_1\|\hat{\mathcal{H}}_{\mathrm{SO\ x}}\|1^3A_2\rangle$	1.27	–0.89	0.94	1.27	–1.27
$\langle 1^3B_1\|\hat{\mathcal{H}}_{\mathrm{SO\ x}}\|2^3A_2\rangle$	–0.73	1.16	–1.13	0.04	–0.02
$\langle 1^3B_2\|\hat{\mathcal{H}}_{\mathrm{SO\ y}}\|1^3A_2\rangle$	0.37	–0.56	–0.55	0.03	0.03
$\langle 1^3B_2\|\hat{\mathcal{H}}_{\mathrm{SO\ y}}\|2^3A_2\rangle$	0.60	–0.40	–0.43	0.76	0.76

[a]: The imaginary unit i has been omitted.

Table S4: Degrees of freedom q_i used in the MCTDH calculations, their harmonic frequencies ω_i (cm^{-1}), number of single-particle-function (n) in multiset formalism, number of Hermitian DVR (N) and induced linear vibronic coupling strength λ (in eV) between nonadiabatic electronic states.

	sym.	label	ω_i	N	n^a	$\lambda_{12}/\lambda_{34}$	$\lambda_{36}/\lambda_{46}$	$\lambda_{35}/\lambda_{45}$	λ_{56}
vacuum	a_1	q_{23}	381.5	35	4/7/5/7/6/6	0.0028/0.0030			
	a_1	q_{138}	1763.2	35		0.0263/0.0268			
toluene	a_1	q_{23}	381.4	35	5/6/5/7/5/6	-0.0036/-0.0019			
	a_1	q_{138}	1751.2	35		0.0243/0.0201			
acetonitrile	a_1	q_{23}	381.1	35	5/7/7/5/6/5	-0.0088/0.0067			
	a_1	q_{138}	1732.0	35		0.0301/0.0217			
vacuum	a_2	q_5	60.0	30	4/4/6/7/4/6		0.0036/0.0025		
	a_2	q_{56}	784.9	30			-0.0235/0.0033		
toluene	a_2	q_5	57.1	30	4/4/7/5/4/6		-0.0078/-0.0193		
	a_2	q_{56}	793.9	30			-0.0244/-0.0236		
acetonitrile	a_2	q_5	63.1	30	4/4/7/5/4/7		0.0154/-0.0030		
	a_2	q_{56}	790.1	30			0.0039/0.0205		
vacuum	b_1	q_{13}	184.6	25				-0.0109/-0.0081	
	b_1	q_{21}	348.7	25	4/4/5/7/7/4			0.0084/-0.0114	
	b_2	q_{26}	427.9	25					-0.0121
toluene	b_1	q_{13}	189.2	25				-0.0032/-0.0079	
	b_1	q_{21}	349.5	25	4/4/7/4/5/4			0.0162/-0.0065	
	b_2	q_{26}	428.0	25					0.0004
acetonitrile	b_1	q_{13}	186.9	25				0.0052/-0.0010	
	b_1	q_{21}	349.8	25	4/4/7/4/6/5			0.0258/-0.0050	
	b_2	q_{26}	428.0	25					-0.0137

[a] 4/7/5/7/6/6 denote the number of SPF for ^{1}(c.t.)/^{1}($n\pi^*$)/^{3}(c.t.*)/^{3}($n\pi^*$)/^{3}(acr.)/^{3}(ant.) states correspondingly.

Figure S1: Most relevant Kohn-Sham BH-LYP MOs at the ground-state geometry in vacuum. They can be grouped into three categories: (1) MOs that are localized on the anthracenone moiety (n_{O}, $\pi_{\mathrm{H-6}}$, $\pi_{\mathrm{H-3}}$, π^*_{L}); (2) MOs that are localized on the acridine moiety ($\pi_{\mathrm{H-2}}$, π_{H}, $\pi^*_{\mathrm{L+4}}$); (3) MOs that are delocalized ($\pi_{\mathrm{H-5}}$, $\pi_{\mathrm{H-4}}$, $\pi_{\mathrm{H-1}}$, $\pi^*_{\mathrm{L+1}}$,$\pi^*_{\mathrm{L+2}}$).

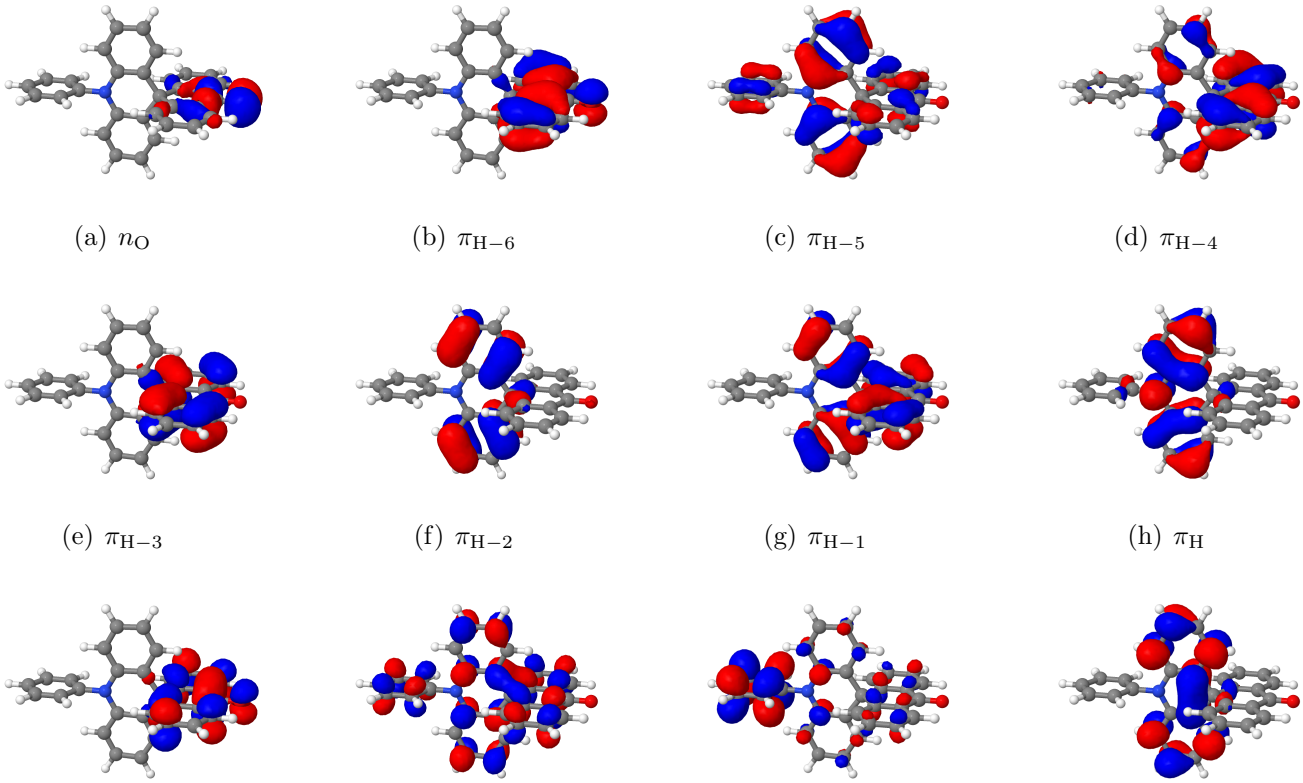

(a) n_{O} (b) $\pi_{\mathrm{H-6}}$ (c) $\pi_{\mathrm{H-5}}$ (d) $\pi_{\mathrm{H-4}}$

(e) $\pi_{\mathrm{H-3}}$ (f) $\pi_{\mathrm{H-2}}$ (g) $\pi_{\mathrm{H-1}}$ (h) π_{H}

(i) π^*_{L} (j) $\pi^*_{\mathrm{L+1}}$ (k) $\pi^*_{\mathrm{L+3}}$ (l) $\pi^*_{\mathrm{L+4}}$

Figure S2: Adiabatic and nonadiabatic 1D potential energy cuts through the distortion coordinates q_i

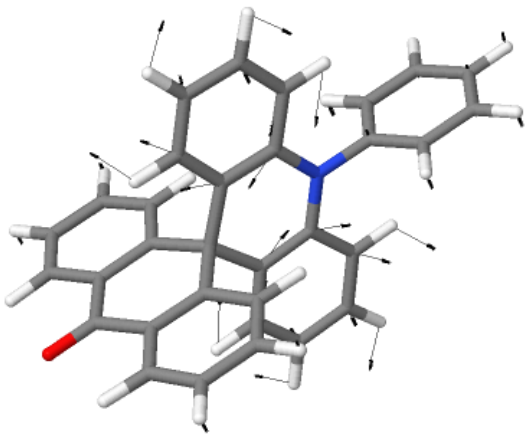

Adiabatic potentials q_{26}

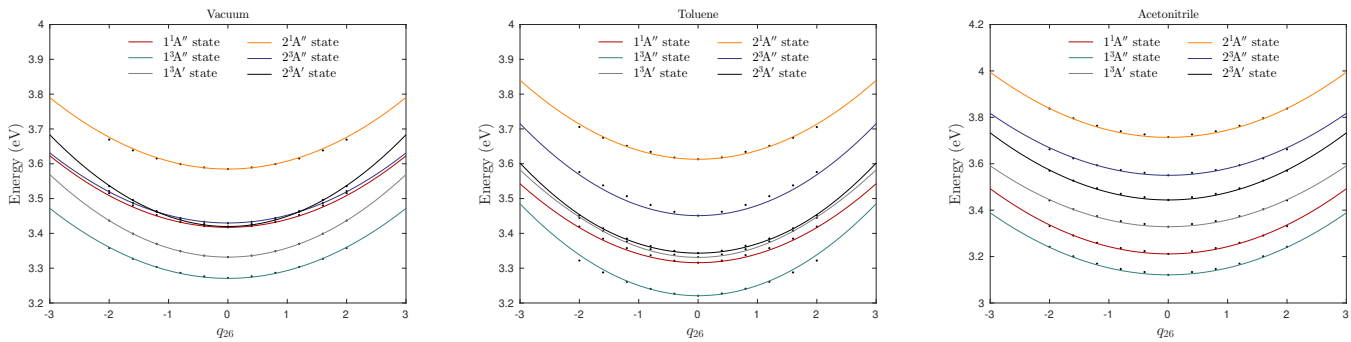

Nonadiabatic potentials q_{26}

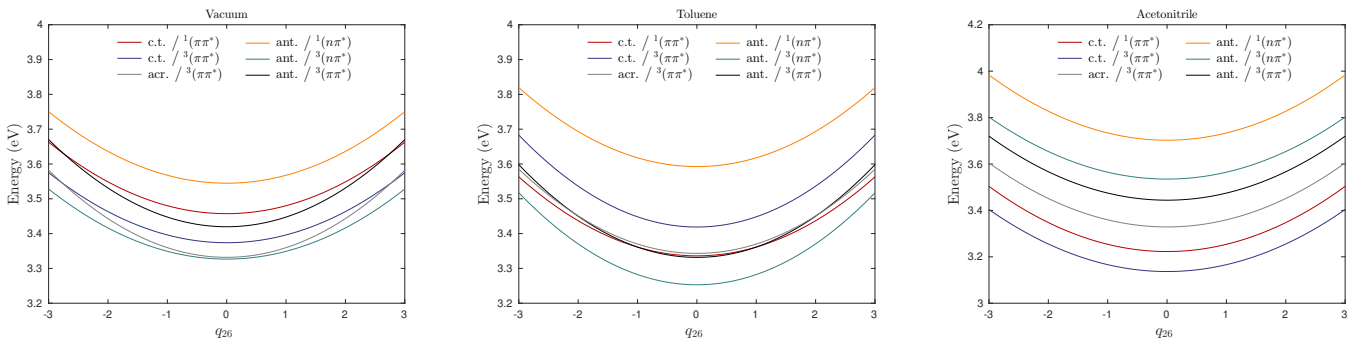

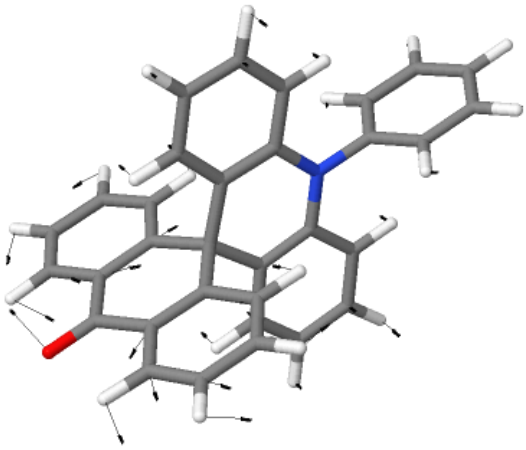

Adiabatic potentials q_{21}

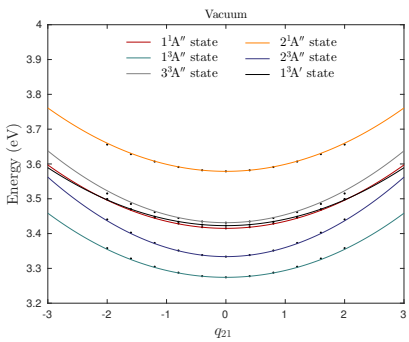

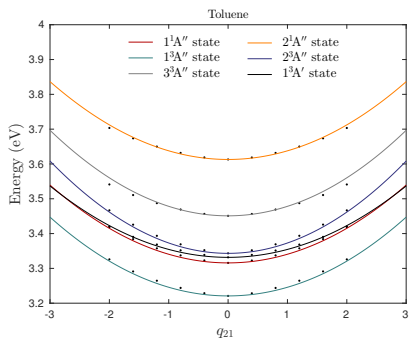

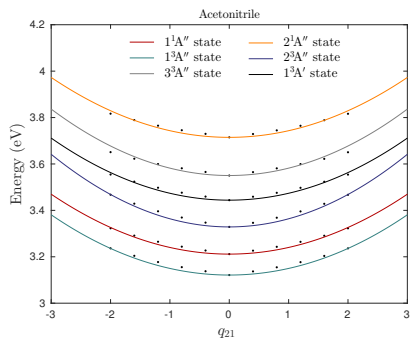

Nonadiabatic potentials q_{21}

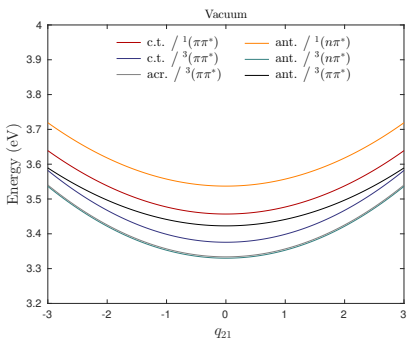

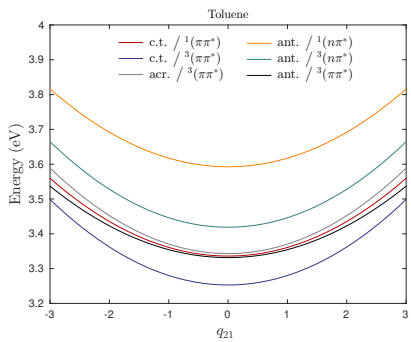

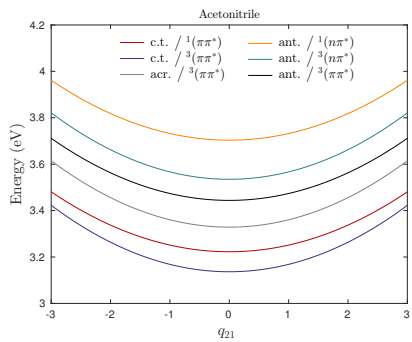

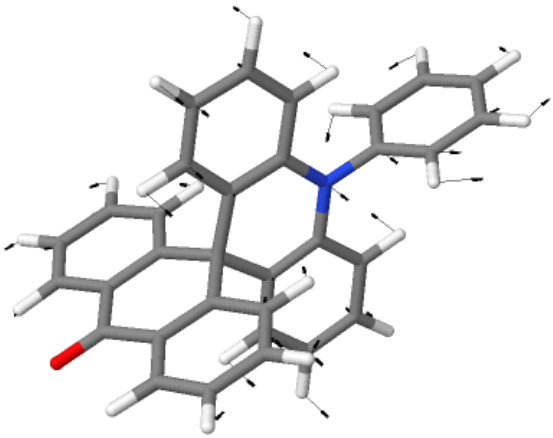

Adiabatic potentials q_{13}

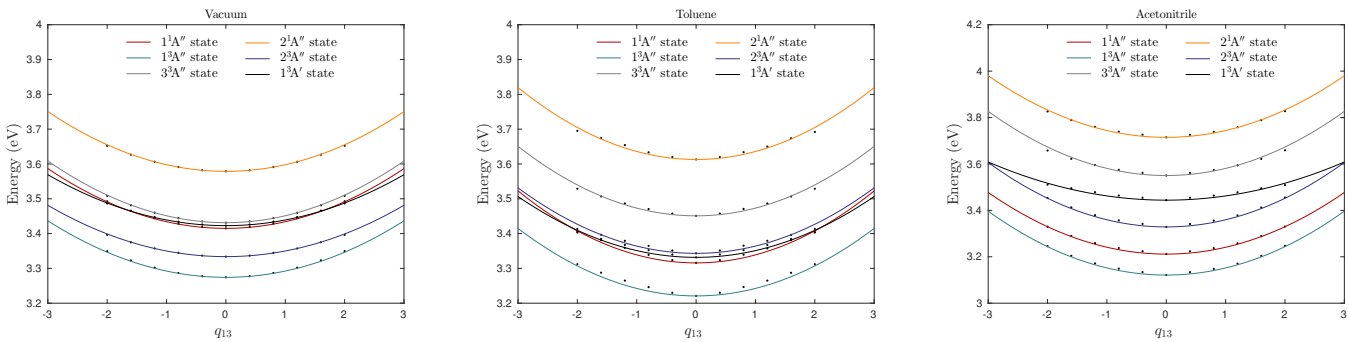

Nonadiabatic potentials q_{13}

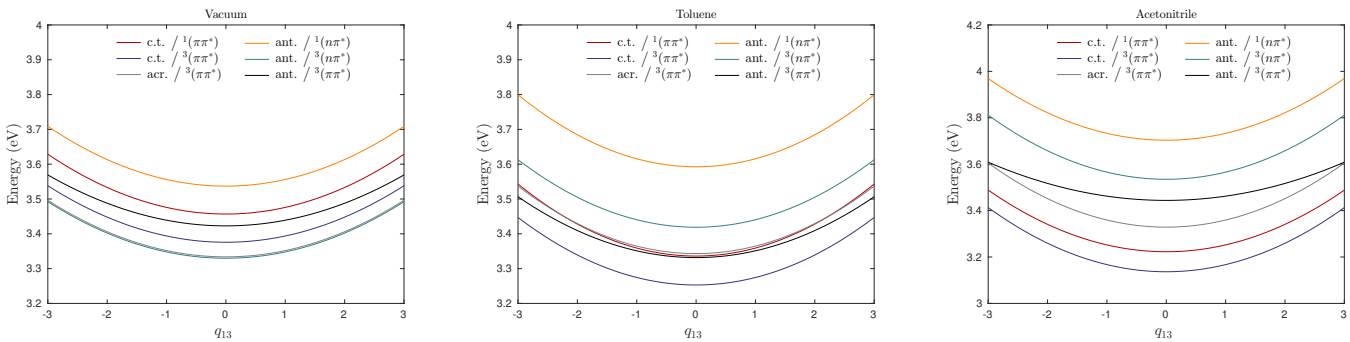

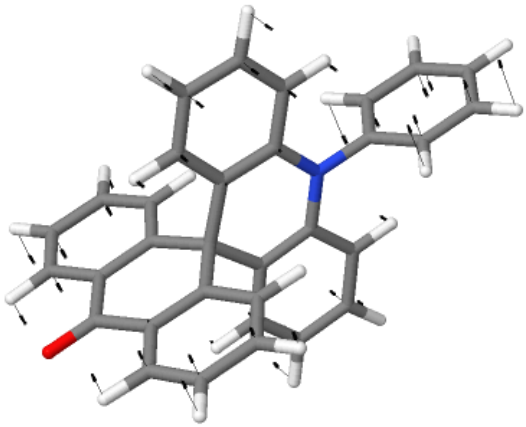

Adiabatic potentials q_5

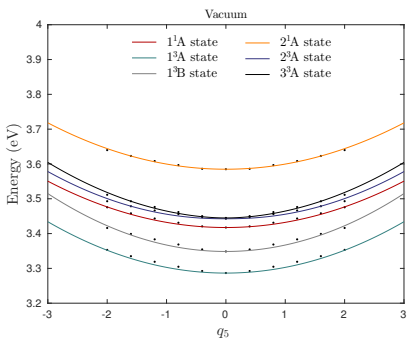

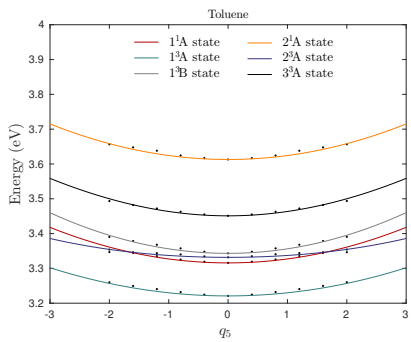

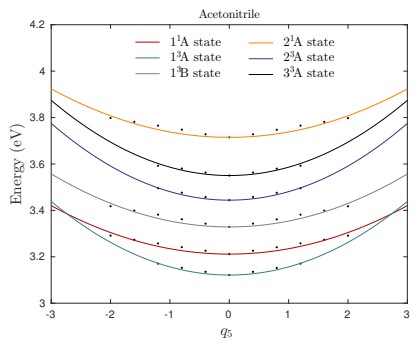

Nonadiabatic potentials q_5

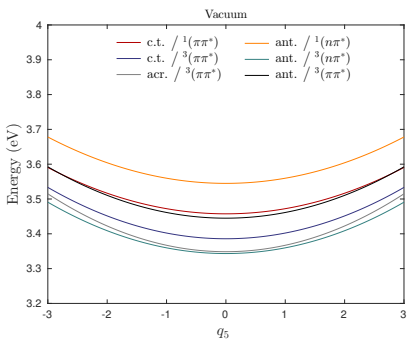

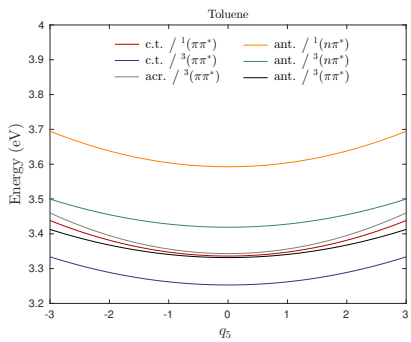

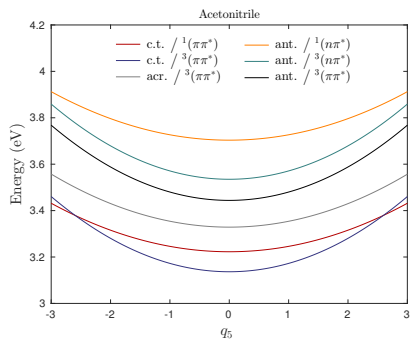

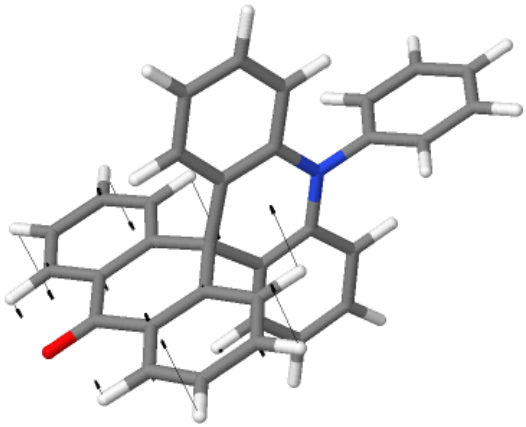

Adiabatic potentials q_{56}

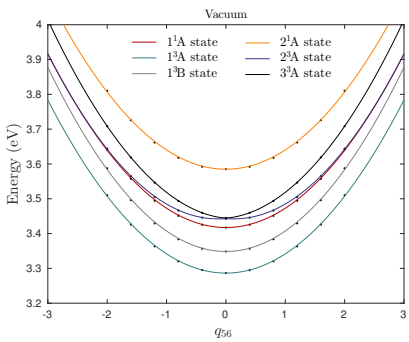

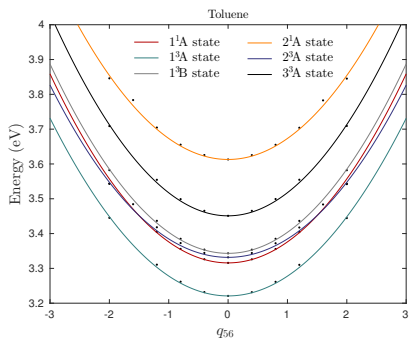

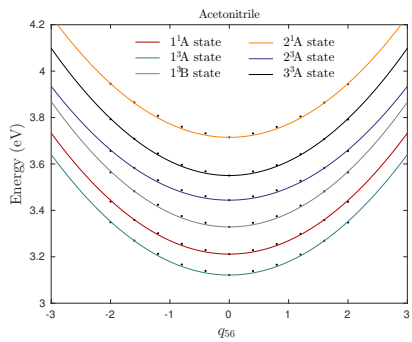

Nonadiabatic potentials q_{56}

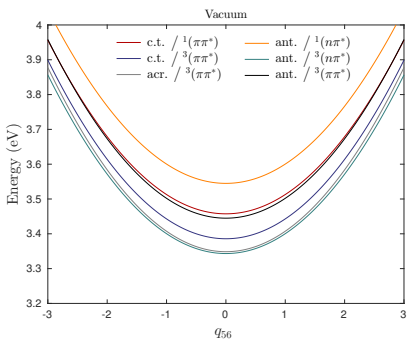

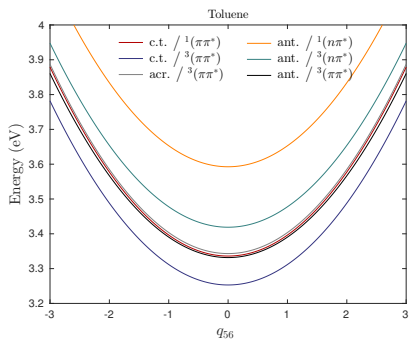

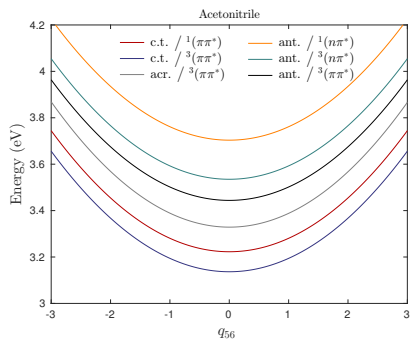

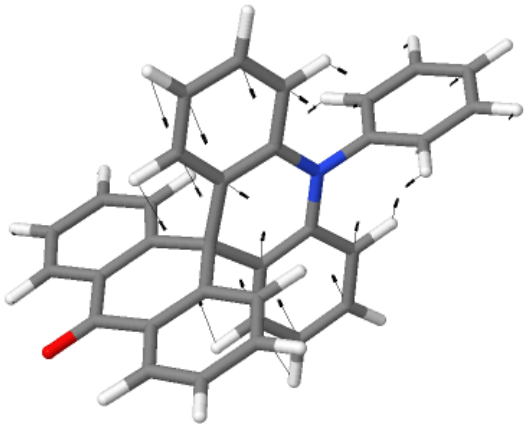

Adiabatic potentials q_{23}

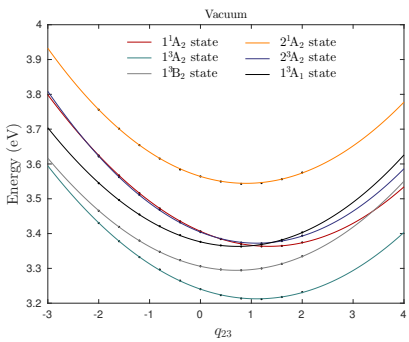

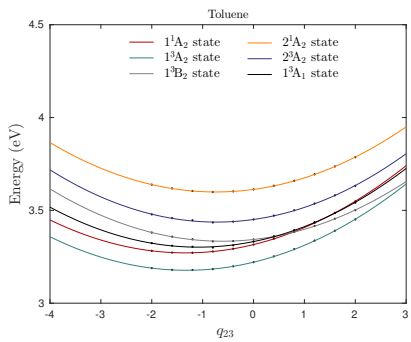

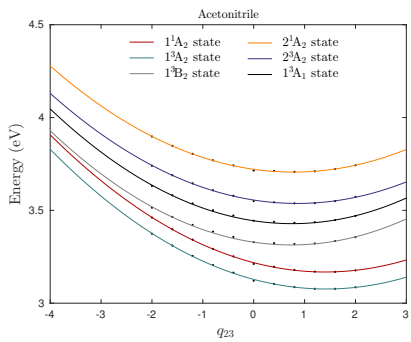

Nonadiabatic potentials q_{23}

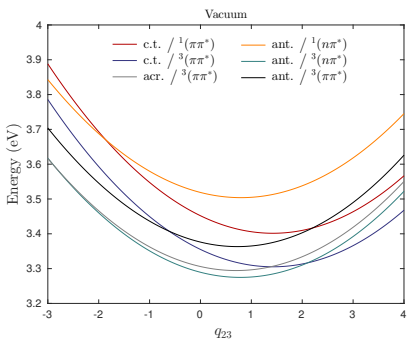

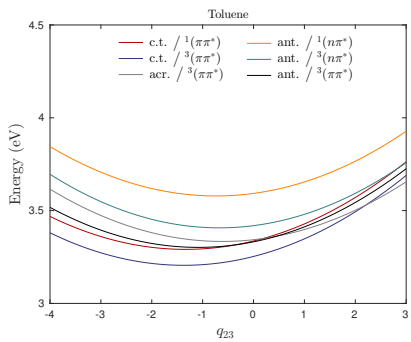

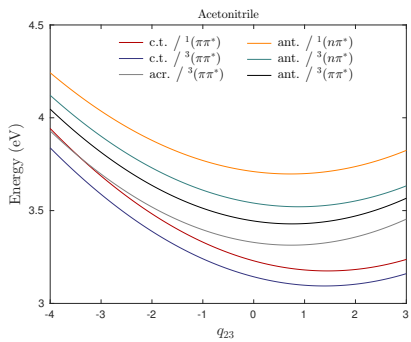

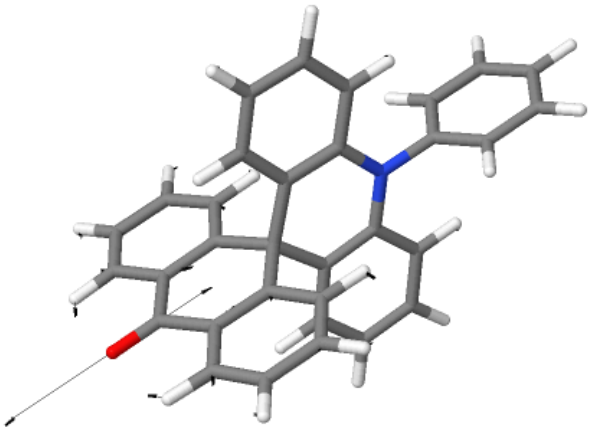

Adiabatic potentials q_{138}

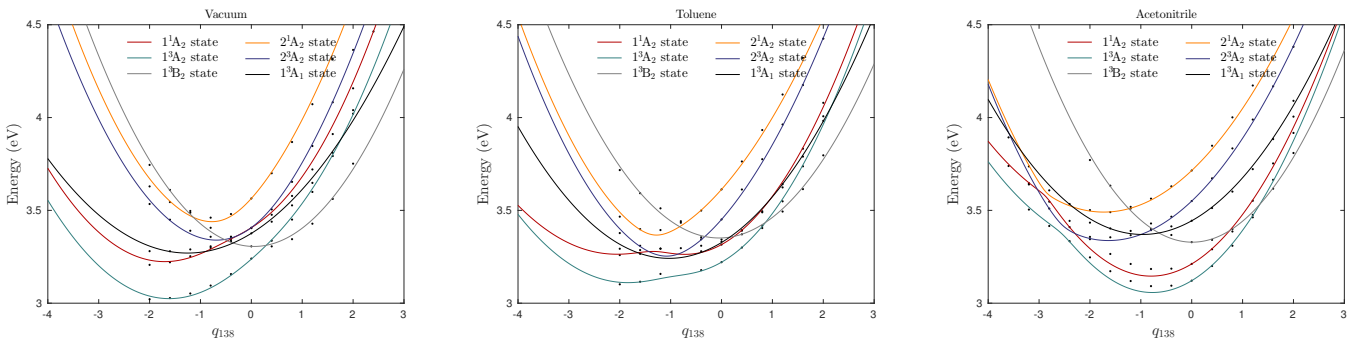

Nonadiabatic potentials q_{138}

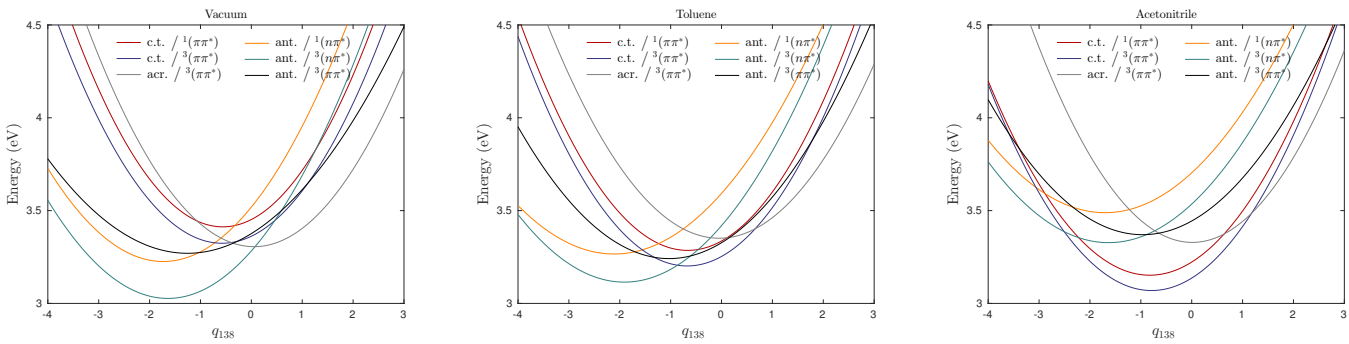

Figure S3: Excited wave packet evolution of ACRSA in vacuum, toluene and acetonitrile.

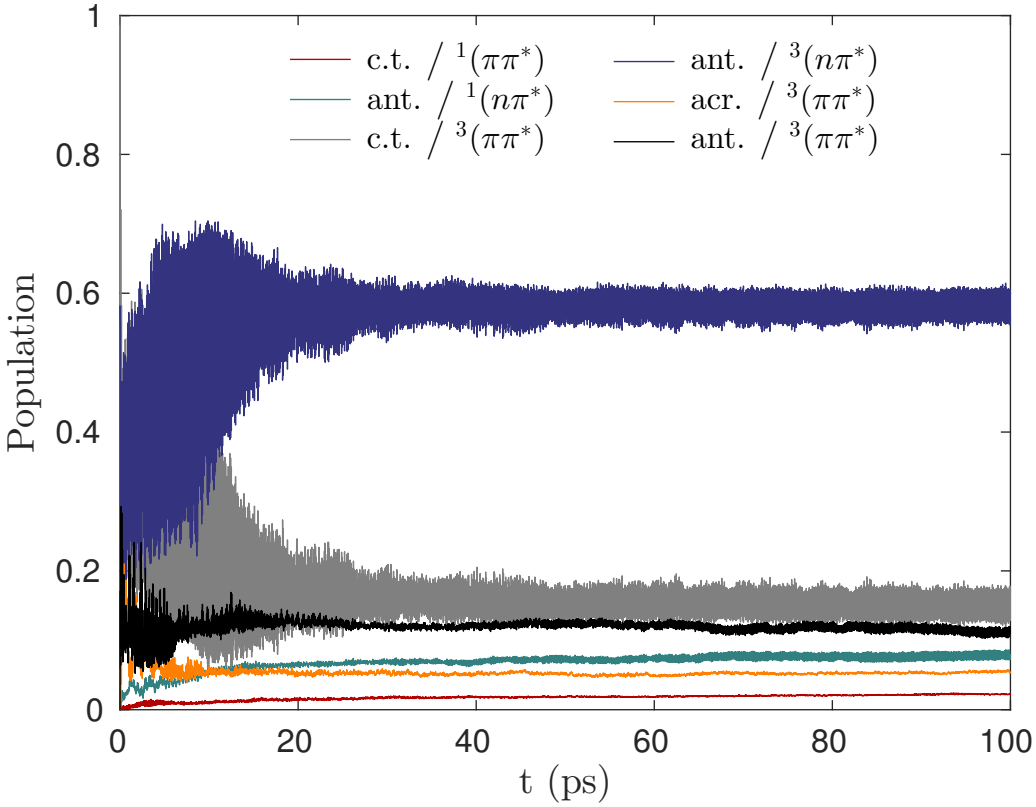

(a) Vacuum

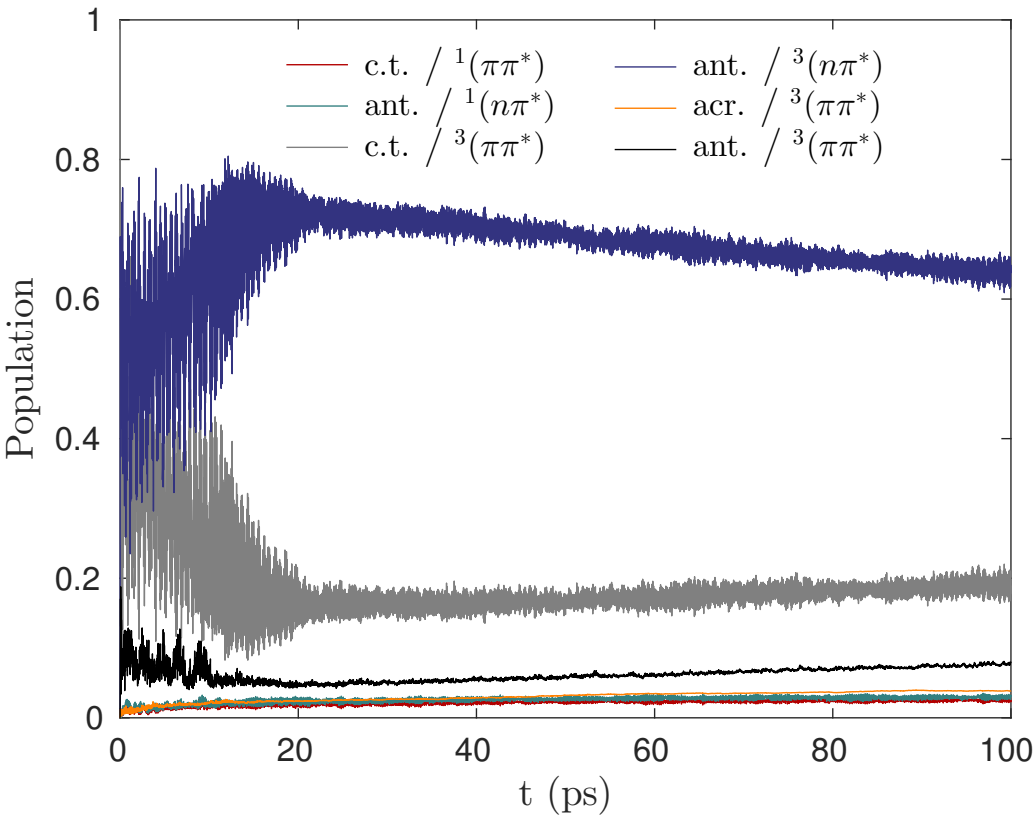

(b) Toluene

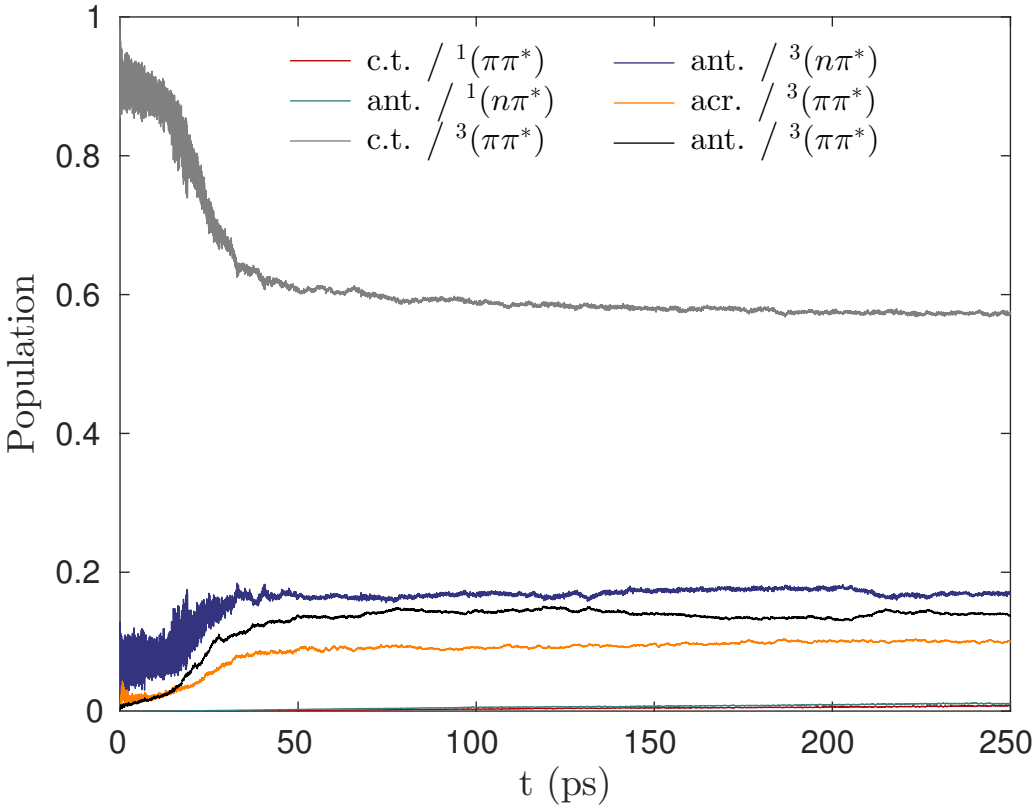

(c) Acetonitrile